

Three-Dimensional Modeling of High-Latitude Scintillation

Alex T. Chartier¹, Biagio Forte², Kshitija B. Deshpande³, Gary S. Bust¹

¹ Johns Hopkins University Applied Physics Laboratory

11100 Johns Hopkins Road

Laurel, MD 21201

USA

² University of Bath

Claverton

Bath, BA2 7AY

United Kingdom

³ Virginia Tech. University

Blacksburg, VA 24061

USA

ABSTRACT

Three-Dimensional Modeling of High-Latitude Scintillation Global Navigation Satellite Systems (GNSS) signals exhibit rapid fluctuations at high and low latitudes, believed to be caused by ionospheric refraction and diffraction. This study focuses on the high-latitude problem, where phase scintillation can cause frequency shifts large enough to result in GNSS receiver loss of lock. At high-latitudes, the ionospheric irregularity region cannot be approximated to a thin layer, so a fully three-dimensional, multiple phase screen modeling approach devised by *Deshpande et al.* [2014] is used. Here, scintillation observations are explained using contemporaneous measurements that specify the large-scale dynamics. Data from EISCAT Incoherent Scatter Radar and SuperDARN HF radar define the macroscopic environment within which irregularities occur, and the small-scale behavior is estimated by varying model parameters. The results support a refractive explanation for the observations in this case, with a ~ 2 km electron density gradient (based on 200 m/s drifts) providing the best agreement.

1. INTRODUCTION

Scintillation is the phenomenon of random phase and amplitude fluctuations in radio signals. Scintillation is seen in transionospheric signals in the frequency range of 100 MHz – 4 GHz [*Basu et*

al., 1988; *Aarons & Basu*, 1993]. The phenomenon is caused by diffractive scattering due to ionospheric irregularities, and refractive lensing due to large-scale electron density gradients. Ionospheric scintillation is observed at both high and low latitudes, though there are differences between the two regions. This study is focused on the high latitude problem, where particle precipitation and magnetospheric convection drive the formation of irregularities. The near-vertical orientation of the geomagnetic field in this region permits thick irregularity layers (> 50 km in altitude) to form.

The likely existence of thick irregularity layers at high latitudes means signal propagation cannot be approximated to transmission through a single thin phase screen. Instead, radio signals are scattered and re-scattered as they travel through the medium. The different components combine, out-of-phase, at the receivers on the ground, resulting in observed signal phase and amplitude fluctuations. The size, shape, altitude, intensity and velocity of the ionospheric irregularities relative to the satellite-receiver line-of-sight all combine to produce the scintillations we observe on the ground. In the refractive case, large-scale electron density gradients move across the line-of-sight causing a focusing and defocusing of the beam that can also be observed as scintillation.

Incoherent scatter radars and other ionospheric remote sensors can observe large-scale electron densities and drifts, but cannot directly resolve the ionospheric structures that cause scintillation. In-situ instruments (e.g. CHAMP) capture the morphology of ionospheric irregularities, typically along satellite tracks, but the coverage required to explain observed scintillation cases does not exist. In this investigation we combine large-scale ionospheric observations with expected irregularity parameters to produce synthetic ionospheres, through which we propagate GPS signals. By matching our model output to the observations, we infer the underlying small-scale ionospheric physics.

2. OBSERVATIONS

In October 2013, an experiment was conducted at Tromsø, Norway, using the European Incoherent Scatter Radar (EISCAT) and a co-located Novatel GSV4004 GPS ionospheric monitor capable of measuring TEC at one-minute intervals, together with 50 Hz signal level and phase [Van Dierendonck *et al.*, 1993]. The EISCAT UHF dish tracked the location of GPS satellite PRN 23, making ionospheric electron density observations along the line-of-sight using the calibrated backscattered power from its 931 MHz transmissions. The dish changed position every 5 minutes, with the satellite moving across it in that period. Initially, five 60-second integrations were made at each location, but *Forte et al.* [2013] found an optimal balance between high time resolution and low uncertainty using 150-second integrations to calculate electron density profiles.

Given the SuperDARN ion velocity observations in the area, we assume a horizontal drift velocity of around 200 m/s, so each 150-second observation equates to around 30 km of ionosphere horizontally. EISCAT electron density observations are shown in Figure 1.

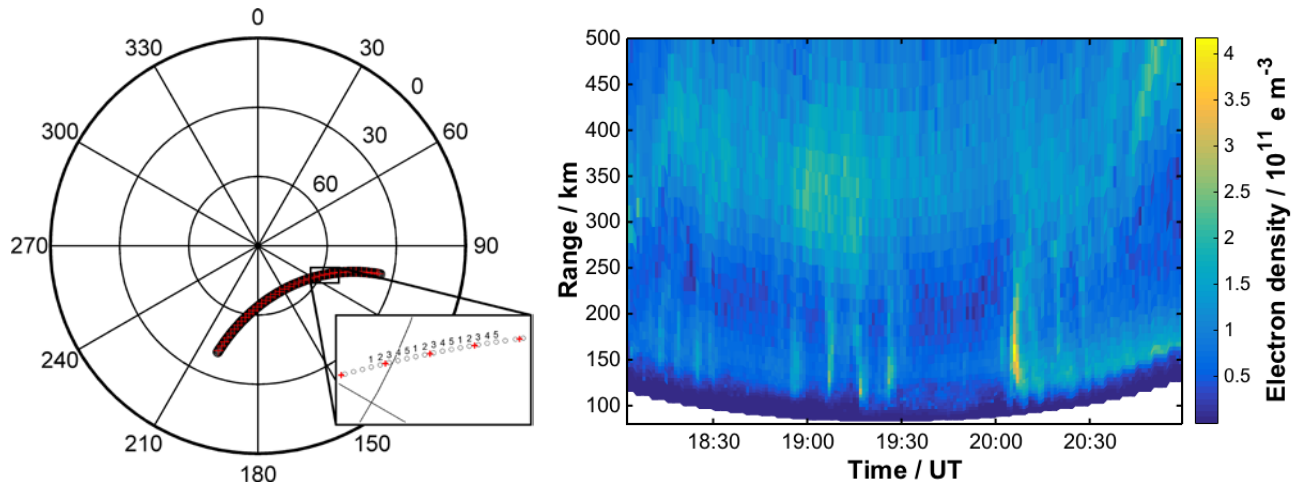


Figure 1: Left: Beam direction. Right: EISCAT electron density observations in the satellite direction, in the evening of 17 October 2013

Figure 1 shows an electron density enhancement at around 20:05 UT. Around this time, rapid phase variations of ~10-second period are seen in filtered phase data from the co-located GPS ionospheric monitor (see Figure 2).

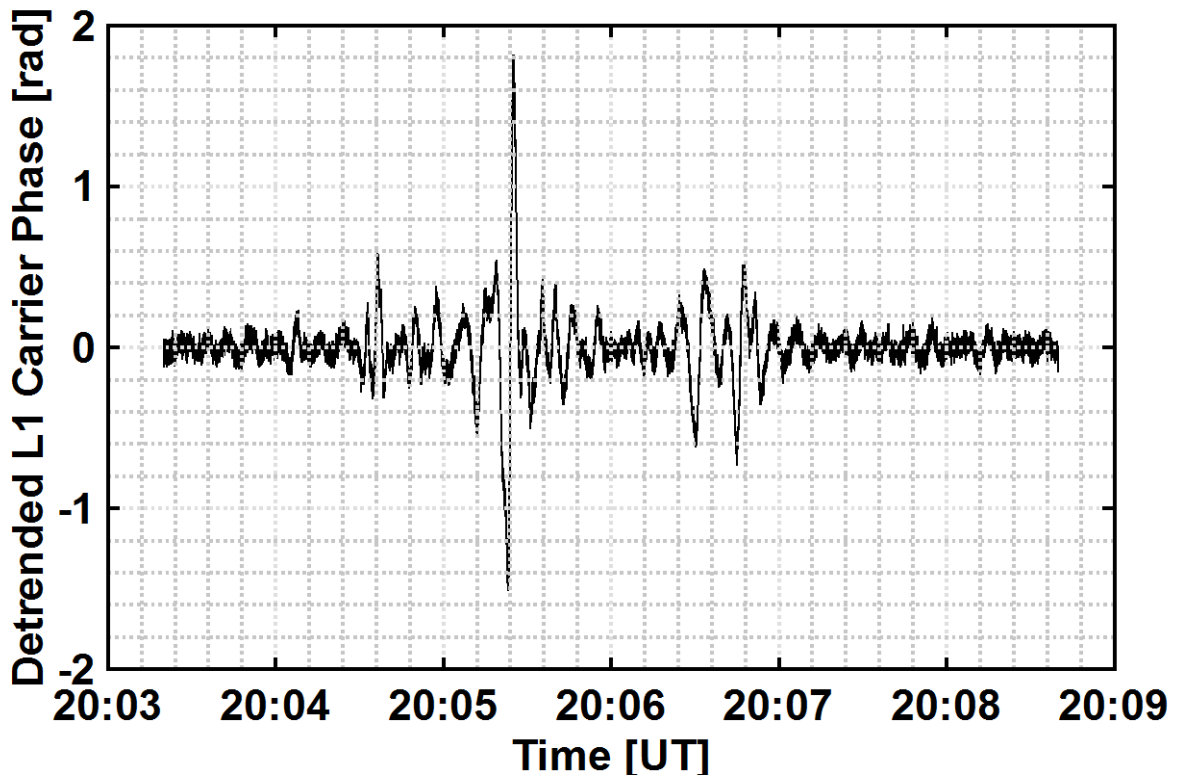


Figure 2: Filtered phase data from the GPS ionospheric monitor at Tromsø, Norway

The large-scale ionospheric electron densities observations from EISCAT are far too coarse to explain the phase activity shown in Figure 2 through refractive or diffractive mechanisms, so a modeling approach is employed to determine the small-scale ionospheric structures. The approach is explained in the next section.

3 MODELING

Deshpande et al. [2014] developed a signal propagation model using a three-dimensional, multiple phase screen approach based on the work of *Rino* [1979]. In this study, the model is adjusted to exploit the unique observational data at our disposal. The model calculates signal propagation through a three-dimensional cuboid of electron densities whose background values are taken from the EISCAT data. That cuboid extends between 100-700 km along the line-of-sight (so long as EISCAT coverage is available), and out 5 km in the perpendicular directions. The cuboid moves to follow the satellite across the sky, removing the need to solve for propagation across a larger, static space. This refinement allows us to use up to 60 phase screens (giving 10 km in-track resolution) in calculating the signal propagation, without requiring excessive computing power. The received signal phase predicted by the model is first unwrapped by removing jumps greater than π , then detrended using a third-order polynomial and finally filtered with a 6th-order Butterworth high-pass filter.

Both refractive and diffractive signal propagation scenarios are explored in an effort to explain the observations. The background ionosphere is represented by a cubic spline interpolation of the EISCAT data (assuming the timesteps are 30 km apart), which then travels across the line-of-sight at 200 m/s. In the refractive scenario, the initial EISCAT timeseries is oversampled so that perpendicular gradients occur over just 2 km. The results are shown in Figure 3.

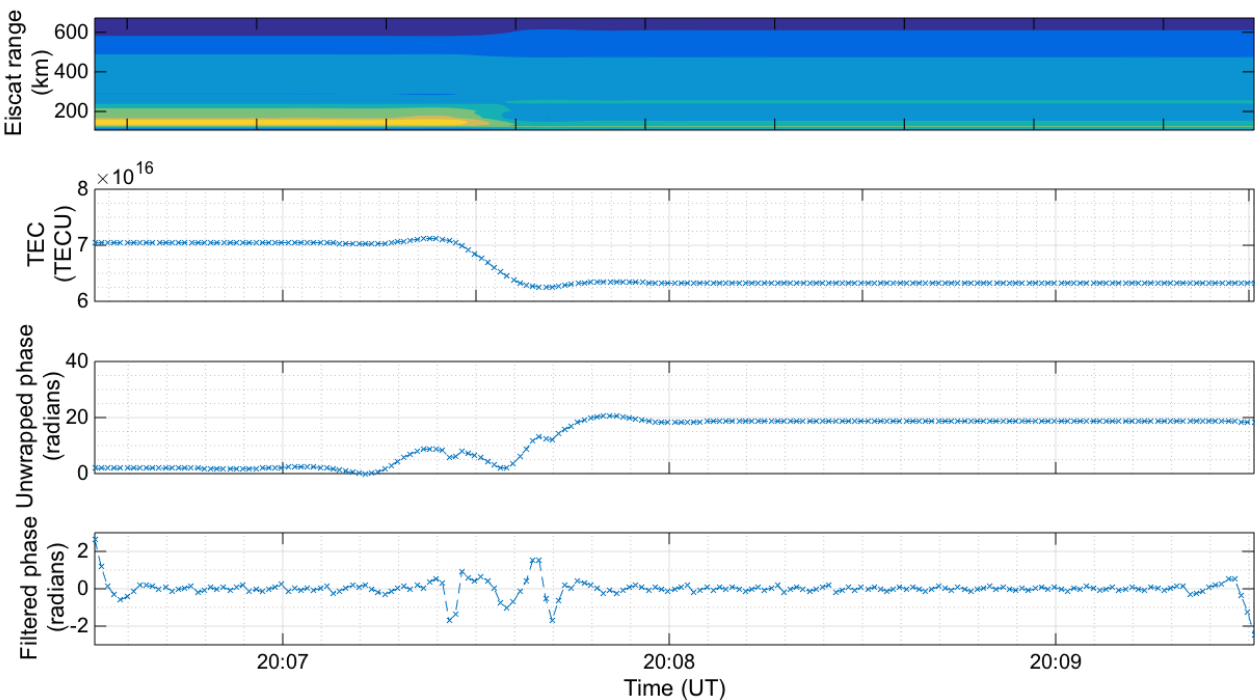


Figure 3 shows (top to bottom) EISCAT electron densities oversampled and cubic spline interpolated to give a 2 km, 200 m/s, second-order smooth gradient in the signal-perpendicular direction; TEC through the electron density representation; unwrapped phase at the receiver; filtered phase at the receiver

The model results (Figure 3) show that this refractive scenario causes phase fluctuations of up to 2 radians lasting about 10-15 seconds. Although not an exact match, this result indicates that the large-scale electron density gradients observed by EISCAT could be sufficient to explain the observations.

The remaining assumption is that density gradients can occur over just 2 km, when the EISCAT resolution is only at the 30 km level (Figure 4).

In the diffractive scenario (Figure 4), large-scale gradients occur over 30 km, but irregularities are added in proportion to the background densities at the 10% level. The irregularity spectrum is formulated according to *Costa & Kelley [1977]*. The axial ratio is set to 5, so that irregularities extend five times further in the direction of the magnetic field than across it. The spectral index is set to 3 and the outer scale is 5 km.

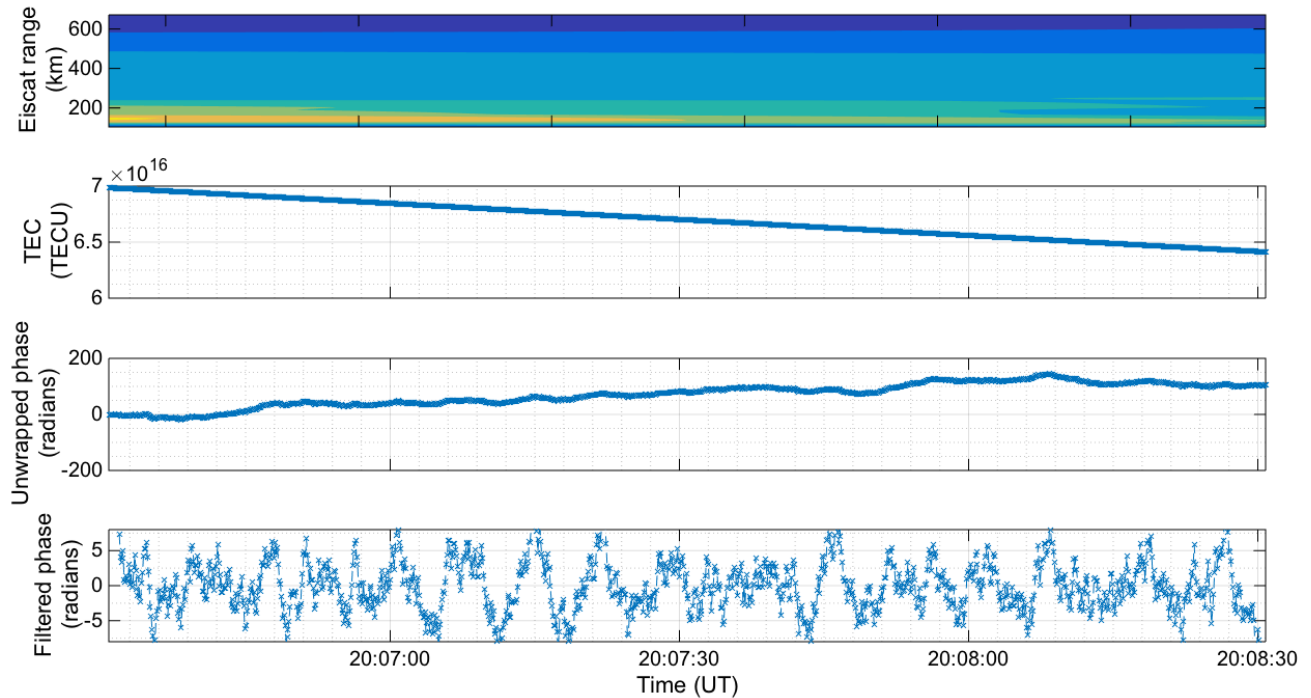


Figure 4 shows (top to bottom) EISCAT electron densities cubic spline interpolated from 150 s (equivalent to 30 km) to 10 Hz (or 20 m) resolution; TEC through the electron density representation; unwrapped phase at the receiver; filtered phase at the receiver

In Figure 4, the model predicts large-amplitude phase fluctuations (± 5 radians) from a typical set of irregularity parameters. The magnitude of this effect is much larger than what is seen in the GPS data.

4. CONCLUSIONS

A GPS ionospheric monitor shows phase fluctuations of ~ 2 radians associated with a large-scale electron density enhancement seen by EISCAT in the ionospheric F-region along the satellite-receiver line-of-sight. A three-dimensional, multiple phase screen modeling approach is developed for this study. The model shows that, given basic assumptions, a refractive mechanism fits the observations better than a diffractive mechanism. We conclude that the observed large-scale electron density gradient is sufficient to explain the observed phase fluctuations, without recourse to any small-scale irregularity mechanisms.

ACKNOWLEDGEMENTS

We acknowledge the support of NSF and the EISCAT ISR facility in pursuing this research.

REFERENCES

- Aarons, J., Basu, S., 1994. Ionospheric amplitude and phase fluctuations at the GPS frequencies. In: Proceedings of ION GPS-94, Arlington, VA, p. 1569.
- Basu, S., MacKenzie, E., Basu, S., 1988. Ionospheric constraints on VHF=UHF communication links during solar maximum and minimum periods. *Radio Science* 23, 363.
- Basu, S., Groves, K. M., Basu, S., & Sultan, P. J. (2002). Specification and forecasting of scintillations in communication/navigation links: current status and future plans. *Journal of atmospheric and solar-terrestrial physics*, 64(16), 1745-1754.
- Costa, E., & Kelley, M. C. (1977). Ionospheric scintillation calculations based on in situ irregularity spectra. *Radio Science*, 12(5), 797-809.
- Deshpande, K. B., Bust, G. S., Clauer, C. R., Rino, C. L., & Carrano, C. S. (2014). Satellite- beacon Ionospheric- scintillation Global Model of the upper Atmosphere (SIGMA) I: High- latitude sensitivity study of the model parameters. *Journal of Geophysical Research: Space Physics*, 119(5), 4026-4043.
- Forte, B., Smith, N. D., Mitchell, C. N., Da Dalt, F., Paniciari, T., Chartier, A. T., Stevanovic, D., Vuckovic, M., Kinrade, J., Tong, J. R., Haggstrom, I. and Turunen, E. (2013) Comparison of temporal fluctuations in the total electron content estimates from EISCAT and GPS along the same line of sight. *Annales Geophysicae*, 31. pp. 745-753. ISSN 0992-7689
- Rino, C. L. (1979). A power law phase screen model for ionospheric scintillation: 1. Weak scatter. *Radio Science*, 14(6), 1135-1145.
- Van Dierendonck, A. J., Hua, Q., and Klobuchar, J.: Ionospheric scintillation monitoring using commercial single frequency C/A code receivers, Proceedings of ION GPS 93, Salt Lake City, UT, 22–24 September, 1333–1342, 1993.